Langmuir

ARTICLE

pubs.acs.org/Langmuir

Patterning Functional Materials Using Channel Diffused Plasma-Etched Self-Assembled Monolayer Templates

Antony George, A. Wouter Maijenburg, Michiel G. Maas, Dave H. A. Blank, and Johan E. ten Elshof*

Inorganic Materials Science Group, MESA+ Institute for Nanotechnology, University of Twente, P.O. Box 217, 7500 AE Enschede, The Netherlands

ABSTRACT: A simple and cost-effective methodology for large-area micrometer-scale patterning of a wide range of metallic and oxidic functional materials is presented. Self-assembled monolayers (SAM) of alkyl thiols on Au were micropatterned by channel-diffused oxygen plasma etching, a method in which selected areas of SAM were protected from plasma oxidation via a soft lithographic stamp. The patterned SAMs were used as templates for site-selective electrodeposition, electroless deposition and solution-phase deposition of functional materials such as ZnO, Ni, Ag thin films, and ZnO nanowires. The patterned SAMs and functional materials were characterized by scanning electron microscopy (SEM), X-ray diffraction (XRD), atomic force microscopy (AFM), and tunneling AFM (TUNA).

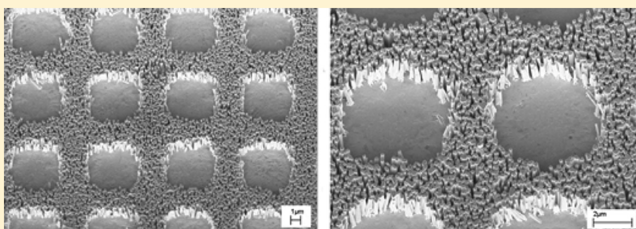

1. INTRODUCTION

Realization of patterns of functional materials is often crucial in all kinds of device fabrication technologies. Over the past two decades, various technologies have been developed for achieving high-fidelity micro- and nanoscale patterns. Technologies that employ patterned self-assembled monolayers (SAMs) of organic molecules such as organosilanes and alkanethiols are very powerful tools in device fabrication due to their ability to act as templates or resists for etching,[1] electrodeposition,[2] and electroless deposition.[3] Patterned SAMs can also be used to add a site-selective local chemical functionality on the surface in order to attach nanomaterials,[4] biomolecules,[5] or polymers.[4]

Several techniques including photolithography,[6] ion beam lithography,[7] electron beam lithography,[1,8] microcontact printing,[9] scanning probe lithographic techniques,[10,11] gas-phase soft lithography,[12] gas-phase pattern deposition,[13] and nanoimprint lithography[4] have been demonstrated for patterning SAMs. The advantage of patterning technologies in which a preformed SAM on a substrate undergoes local destruction or chemical modification by photo-oxidation, focused ion beam (FIB) or e-beam lithography (EBL), is the high quality of the final SAM pattern, because the formation of SAMs from the liquid or gas phase is known to yield densely packed SAMs with a low defect density. Scanning probe techniques such as nanoshaving[14] can also be used to pattern SAMs by displacing the self-assembled molecules from selected regions. However, the serial nature of processes like EBL, FIB, and scanning probe techniques limits their application window enormously, even though these methods can produce extremely high resolution patterns. In comparison, the more commonly used microcontact printing technique can fabricate patterned SAMs directly in a potentially up-scalable patterning process, but the controlled release of ink molecules to the substrate from the elastomeric poly(dimethylsiloxane) (PDMS) stamps leads to SAM patterns with a relatively higher defect concentration. Problems such as loss of fidelity due to ink diffusion in lateral direction may occur, which sets a limit on the contact pressure, contact duration, and ink concentration in microcontact printing processes.[15−17]

Koumoto and co-workers used a photo-oxidation technique to micropattern preformed SAMs by modifying the chemical functionality of the SAM end groups via exposure to UV light through photomasks.[18−23] They used patterned SAMs as templates for site-selective solution-phase or gas-phase deposition of functional materials such as ZnO, SnO_2, and TiO_2 by selectively adsorbing or precipitating materials,[19−21] or by electroless deposition by binding Pd catalyst on the oxidized regions of the substrate.[22,23] The technique was studied thoroughly and has proven its ability to pattern a wide range of functional materials on the micrometer scale. However, the technique can only be used for local chemical modification of the SAM, but is not suitable for complete uniform destruction of the SAM in order to expose the underlying substrate.

Recently, Lin et al. introduced another novel "ink-free" approach to pattern SAMs via channel diffused plasma surface modification.[24] In this technique, the channels formed between a PDMS stamp and a SAM-coated substrate are used to guide oxidizing plasma to selected areas where the SAM has to be etched or modified. The plasma is spatially controlled inside the channels, and only the patches of SAM that are directly exposed to the plasma are modified. The method provides easy nanometer-to-millimeter-scale nanopatterning of SAMs over large surface areas. The method is faster than photo-oxidation, EBL, FIB, and scanning probe techniques, and does not have the limitations of microcontact printing with respect to pattern resolution.

Received: April 14, 2011
Revised: June 8, 2011
Published: August 22, 2011

 © 2011 American Chemical Society

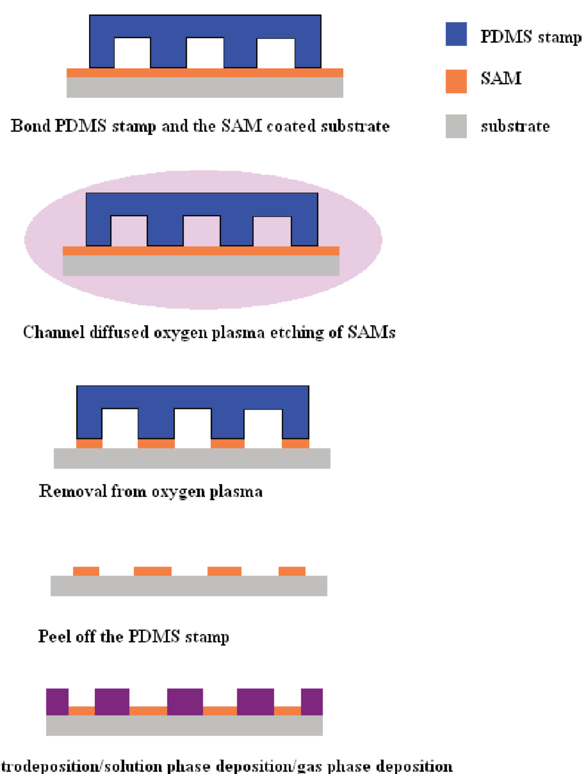

Figure 1. Schematic diagram of the channel-diffused plasma patterning process.

In the present paper, we demonstrate the micropatterning of a wide range of functional metallic and oxide materials such as Ni, Ag, ZnO, and vertically aligned ZnO nanowires via the channel-diffused plasma surface modification technique. A schematic diagram of the patterning process is shown in Figure 1. First, conformal contact is made between the PDMS stamp and the SAM-coated substrate. The substrate is a gold-covered silicon substrate with an octadecanethiol (ODT) SAM. The substrate-stamp assembly is then exposed to oxygen plasma. The oxidizing plasma diffuses into the PDMS channels and oxidizes the part of the SAM that is exposed to the plasma. The regions on the substrate that are in conformal contact with the protruding parts of the PDMS stamp are protected from etching. After plasma exposure, the PDMS stamp is peeled off the substrate and functional materials are selectively patterned via electrodeposition, electroless deposition, and solution-phase deposition.

2. EXPERIMENTAL SECTION

2.1. Preparation of PDMS Stamps. PDMS and curing agent (Sylgard 184) were purchased from Dow Corning Corporation and mixed in a mass ratio 10:1 and poured over the micro/nanopatterned silicon master (created by photolithography or e-beam lithography). The PDMS was cured for 48 h at 70 °C. After curing, the PDMS stamps were removed from the master and cut into pieces of approximately 8 × 8 mm^2 size.

2.2. Preparation of Au-Coated Silicon Substrates. p-Type silicon substrates cleaned with piranha solution (a mixture of H_2O_2 and H_2SO_4 in 1:3 volume ratio) were used in the experiments. The substrates were washed several times with deionized water and stored in deionized water. Prior to use, the substrates were blown dried in a nitrogen stream. Au films with a thickness of 10 to 75 nm were prepared on silicon substrates using a Perkin-Elmer sputtering machine operating at 50 W at a deposition pressure of 2×10^{-5} mbar using Ar as sputtering gas.

2.3. Preparation of ODT-SAM on Au, Thin Films. 1-Octadecanethiol (ODT, purity 97%) was purchased from Sigma-Aldrich and used for self-assembly. ODT SAMs on Au were prepared by soaking the substrate in a 0.5 M solution of ODT in ethanol for 12−48 h. After SAM deposition, the substrates were taken out of the solution and washed in absolute ethanol and dried in a stream of nitrogen and stored for further use.

2.4. Channel Diffused Plasma Etching of SAMs. The PDMS stamps with micro/nanopatterned features were gently pressed against the SAM-coated substrates. The patterned side of the stamp faced the SAM-coated side of the substrate. The PDMS stamp made conformal contact with the substrate via attractive van der Waals forces. The substrate−stamp assembly was transferred to an oxygen plasma cleaner (Harrick Plasma) operating at 25 W at a pressure <1 mbar. The substrates were exposed to oxygen plasma for 20 min. After plasma etching, the PDMS stamp was peeled off the substrate and the substrate was stored until further use.

2.5. Electrodeposition of ZnO and Ni. ODT-SAM patterned Au thin films with an Au layer thickness of ∼75 nm were used as substrate for electrodeposition. Electrodeposition was carried out using a three-electrode potentiostat (Autolab PGSTAT 128N, Metrohm Autolab, Netherlands). The SAM-patterned substrates were used as working electrodes. A small Pt mesh was used as counter electrode. The reference electrode was Ag/AgCl in 3 M KCl (Metrohm Autolab). Nickel patterns were formed from an electrolyte containing 0.23 M nickel sulfate hexahydrate ($NiSO_4 \cdot 6H_2O$, Sigma-Aldrch, purity 99%,) and 0.15 M boric acid (H_3BO_3, Aldrich, purity 99.99%). Deposition occurred at −1.00 V versus reference. Zinc oxide patterns were formed at 70 °C at −1.00 V in an electrolyte containing 0.10 M zinc nitrate hexahydrate ($Zn(NO_3)_2 \cdot 6H_2O$, Sigma-Aldrich, purity 98%). Further details can be found elsewhere.[36]

2.6. Electroless Deposition of ZnO. Electroless deposition of ZnO was carried out as described in ref 25. An ODT-SAM-patterned thin Au film of ∼10 nm thickness was used as substrate. 1.5 g of Zinc nitrate hexahydrate and 0.058 g of dimethylamine borane (DMAB, Aldrich, purity 97%) were dissolved in 100 mL water. The solution was heated to 55 or 65 °C, and the substrates were immersed in the solution for 15 min up to a few hours for ZnO thin film growth.

2.7. Deposition of Silver. Ag deposition solutions (Silver enhancer A and Silver enhancer B) were obtained from Aldrich and mixed in equal proportions. The solution was diluted with water to 25%. The ODT-patterned Au substrates were placed in the solution for few minutes for Ag film growth.

2.8. Solution-Phase Growth of Vertically Aligned ZnO Nanowires. An ODT-SAM patterned thin Au film of ∼10 nm thickness was used as substrate. Hexagonal ZnO seeds were grown at 65 °C for 15 min on the Au patches of the substrate by exposing the substrates to the solution used for thin film growth as described in section 2.6. After seeding, ZnO nanowires were grown on the substrate as described in more detail in ref 26. $Zn(NO)_3 \cdot 6H_2O$ (0.15 g) and 0.07 g of hexamethylenetetramine (HMTA, Fluka, purity 99.5%) were mixed in 100 mL water. The solution was heated to 70−85 °C. The substrates were then placed floating upside-down on the surface of the ZnO growth solution. ZnO nanowires were grown for 2 to 15 h, depending on the desired length of the nanowires.

2.9. Characterization. SAM patterns were characterized using tapping-mode atomic force microscopy (AFM; Veeco Dimension Icon) to determine the surface morphology. Tunneling current AFM (TUNA) was used to study the conducting properties of the grown patterns, as well as to map the conductivity of patterned surfaces.[37] Grown metal and oxide patterns were imaged using high-resolution scanning electron

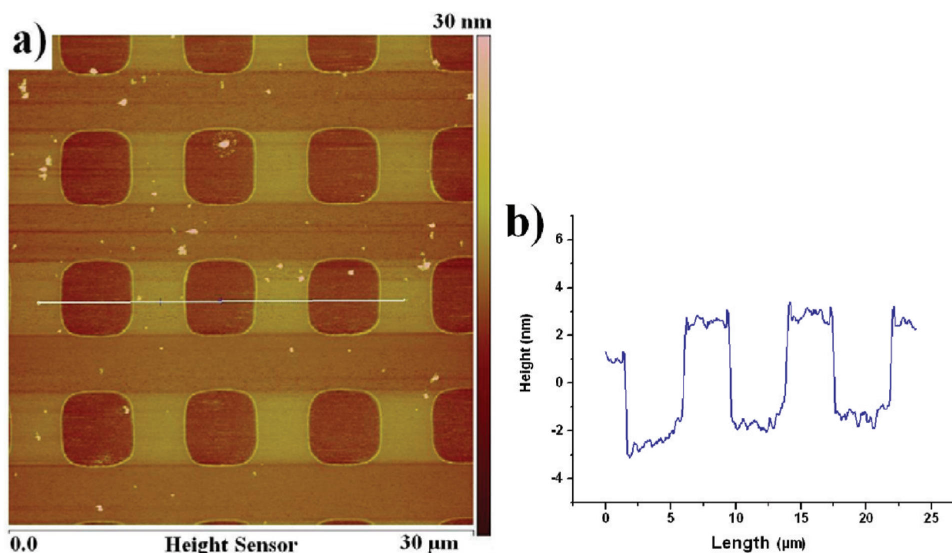

Figure 2. (a) AFM height image and height profile of ODT-SAM on Au substrate. The square pattern containing the SAM has a size of 5.2 μm and the spacing between the squares is 2.8 μm. (b) The height−distance plot shows that the etched regions are elevated with respect to the SAM-covered regions. The white line in (a) indicates the exact trajectory that is plotted in (b).

microscopy (HR-SEM, Zeiss 1550) and tapping-mode AFM. X-ray diffraction (XRD, Philips defractometer PW 3020, software *XPert Data Collector* 2.0e, Panalytical B.V., Almelo, The Netherlands) was used for phase determination of the patterns.

3. RESULTS AND DISCUSSION

3.1. Channel-Diffused Plasma Patterning of SAMs. Oxygen plasma treatment is a common technique to clean substrates[27−29] or chemically modify plastic surfaces to induce hydrophilicity.[27] In soft lithographic techniques like micromolding in capillaries (MIMIC) and microtransfer molding (μTM), oxygen plasma is used to increase the surface energy of the PDMS surface to improve the wetting and promote the flow of sol−gel precursor solutions in PDMS channels.[28,29] In the present paper, we exploited the fact that the hydrocarbon chains of the alkanethiols and organosilane SAMs are oxidized by the plasma.

Figure 2a shows tapping-mode AFM images of a patterned ODT-SAM on an Au substrate. The squares indicate the areas where the PDMS stamp was in conformal contact with the substrate. The SAM in that region was protected from exposure to oxygen plasma. The square patterns have a size of 5.2 μm and the spacing between the squares is 2.8 μm. The AFM height−distance plot shown in Figure 2b indicates that the plasma-modified regions are elevated by ~3 nm with respect to the nonmodified SAM covered regions. We think that exposure of the Au surface to plasma affected the atomic packing in the close-packed structure of the Au film locally, so that the film density decreased and the Au film was lifted up slightly. To confirm this hypothesis, we plasma-patterned an OTS monolayer on a native oxide-coated silicon substrate and determined the local heights on the substrate. No height increase of regions that had been exposed to the plasma was observed in this case. This is attributed to the chemical resistance of the native oxide layer.

The plasma diffusion process inside the channels is time- and geometry-dependent.[24] We found that the etching time for the complete removal of SAMs in an area of about 6 × 6 mm^2 is ~15 min. However, a substantial degree of chemical modification can already be accomplished by partial oxidation over an area of 1 × 1 cm^2 within 10 min of exposure time. Large area patterning is possible using multiple stamps. We found that the stamps can be used for many patterning cycles without any loss of quality of the replicated patterns. We examined various PDMS stamp pattern geometries including straight lines and interconnected network-type channel structures such as square grids, circular grids, and honeycomb-type channel arrays. Optical microscopy examination confirmed that relatively long exposure times were required for complete oxidation of SAMs in unconnected channel structures (straight lines, zigzag lines, bent lines, etc.) when compared to pattern geometries derived from interconnected channel structures. We also examined PDMS stamps with different height-to-width aspect ratios to determine the dependence of the plasma diffusion rate on aspect ratio. PDMS channels with a larger aspect ratio allowed faster diffusion of plasma, so that substantial diffusion distances could be accomplished in less time.

3.2. Deposition Experiments. *3.2.1. Electroless Deposition of ZnO Thin Films.* ZnO thin films were deposited on SAM-etched regions following the recipe of Izaki and Omi as explained in section 2.3.[25] The film growth mechanism is explained in detail in ref 25. Figure 3 shows various ZnO patterns grown on the etched regions of the substrate. The plasma-roughened Au patches were more hydrophilic than the hydrocarbon end groups of the SAMs. The hydrophilicity and roughness promoted the nucleation of ZnO on these areas, and their subsequent growth into thin films. To show the versatility of the technique, we used different pattern geometries, including lines, dots, grids, and honeycomb patterns. The SEM images in Figure 3 show that nucleation took place only within the etched regions of the substrate. No deposition of ZnO was observed on the SAM-covered regions even after 3 h of reaction.

It was also possible to fabricate isolated ZnO patterns when a slightly modified procedure was adopted. A PDMS mask with an interconnected square channel structure was used. After the plasma etching step, a Au etching step was introduced to remove the Au film from all plasma-etched areas. This yielded a pattern of isolated square Au patches on the substrate. The SAM was removed

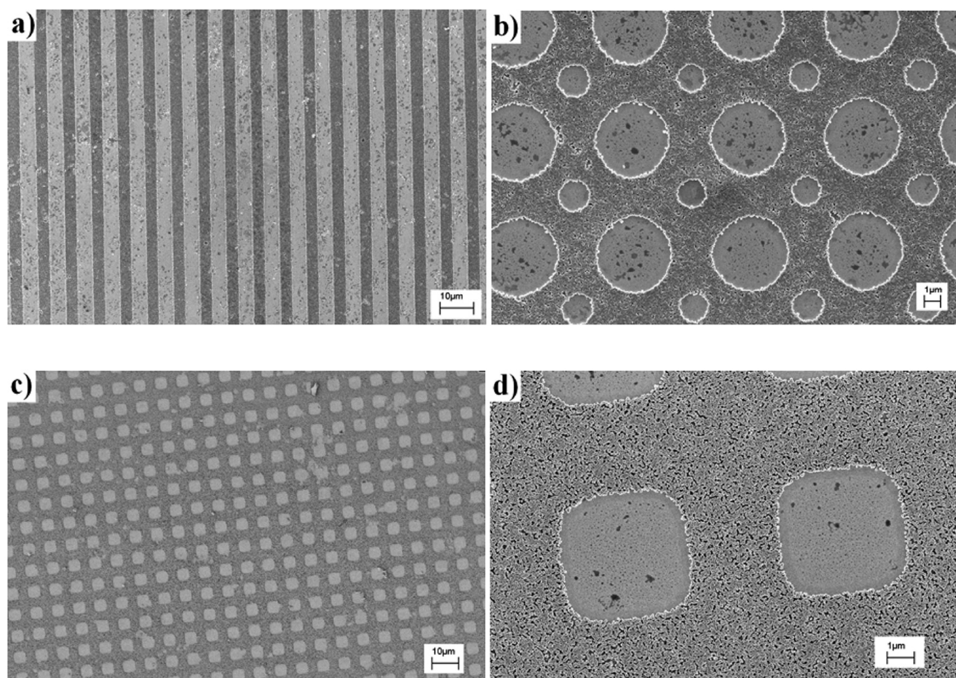

Figure 3. SEM images of ZnO patterns formed by area-selective electroless deposition on Au-covered regions of the substrate. All patterns were grown for 1 h and have a thickness of ~200 nm. (a) Line pattern (width 3.5 μm; spacing 4.3 μm). (b) Pit-patterned ZnO film (diameter large circles 4.5 μm; diameter small circles 2.5 μm; minimum spacing between circles ~2 μm). (c) Square-patterned film (width 5.2 μm; spacing 2.8 μm); (d) Magnified image of the square-patterned film in (c).

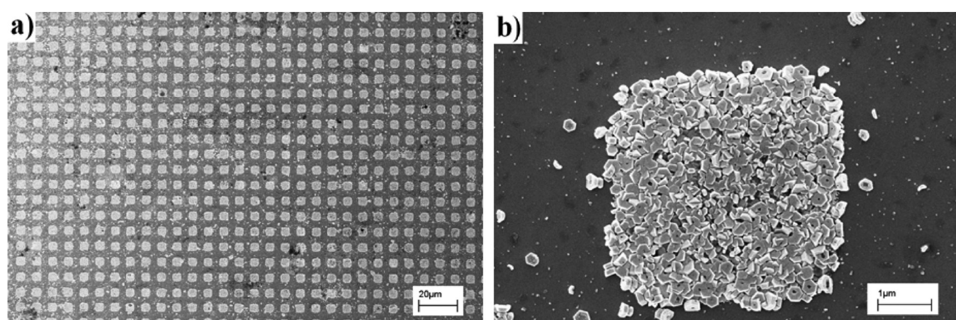

Figure 4. (a) Square array of ZnO square dots on-Au patterned silicon oxide substrate. (b) Magnified view showing a high concentration of ZnO nuclei on Au patches, and a low concentration of ZnO nuclei on the surrounding SiO_x substrate.

by a second exposure to plasma of the entire substrate. ZnO was grown by electroless deposition on the Au patches. The resulting ZnO square dot array on silicon is shown in Figure 4a. The polarity of the native silicon oxide layer is higher than that of the ODT SAM. The hydrophobic−hydrophilic contrast of Au-patterned SiO_x substrates is therefore lower than on ODT-patterned Au substrates, which is why some isolated ZnO nuclei are found on the bare SiO_x areas of the substrate, as illustrated in Figure 4b.

Figure 5 shows the AFM height profile corresponding with the ZnO patterned substrate of Figure 4. The deposition time was 1 h. A ZnO film of ~200 nm thickness formed on the patterned Au patches. Figure 6 shows the ZnO film thickness as function of deposition time. The rate of deposition was approximately 3−4 nm/min, independent of deposition time. However, the SEM images showed that during the initial 15−30 min of film growth the film density was not uniform. Longer deposition times yielded more uniformly covered films. Figure 7a,b shows the surface morphology of films grown at 55 and 65 °C, respectively.

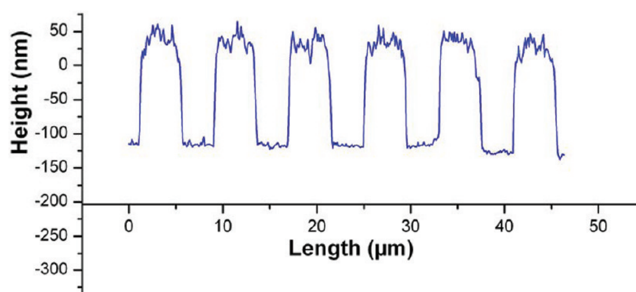

Figure 5. AFM height profile of ZnO square grid patterns after 1 h of deposition time. The film has a thickness of ~200 nm, with a surface roughness of 40 nm.

The films grown at 55 °C were continuous and dense. At 65 °C, individual hexagonal ZnO crystallites with a preferential orientation perpendicular to the substrate grew on the Au film. Their crystal structure was analyzed by XRD. Figure 8 shows the XRD pattern of ZnO thin films grown at 65 °C. The peak at $2\theta = 34.5°$ corresponds to the (0002) orientation of the wurtzite crystal structure. This indicates preferentially (0001) oriented growth of the ZnO films, in agreement with the columnar structure that is visible in Figure 7b.

The conductivity of these patterns was characterized via tunneling AFM (TUNAFM). Figure 9a,b shows a contact-mode AFM image, TUNA conductivity map, and TUNA $I-V$ characteristics of isolated ZnO patterns obtained via electroless deposition. The contact-mode image and conductivity map were recorded simultaneously with an applied sample bias of 3 V versus the AFM tip. The data show uniform conductivity of the ZnO patterns. The shape of the $I-V$ curve is characteristic of semiconducting materials, and illustrates the semiconducting character of the ZnO patterns. In order to obtain consistent data, the $I-V$ characteristics were recorded at several locations. Furthermore, to exclude the possibility that the conductivity of the silicon substrate is measured instead of the sample, $I-V$ characteristics were also measured on the silicon substrate and no conductivity was observed during the measurements.

3.2.2. Patterning ZnO Nanowires. ZnO nanowires are important nanostructures with many potential applications in the fabrication of devices such as nanogenerators,[30] nanophotonic devices,[31] gas sensors,[32] solar sells,[33] field emission devices,[34] and biosensors.[35] The fabrication of vertically aligned ZnO nanowires is very important for many device component applications.

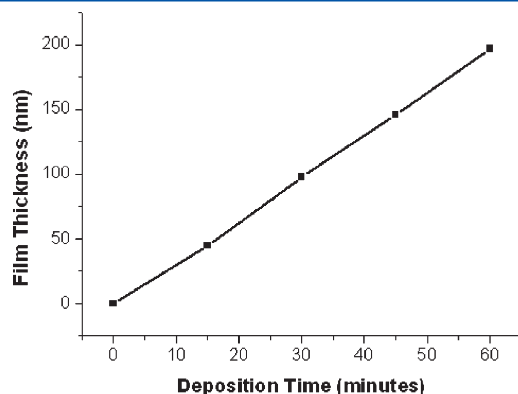

Figure 6. Film thickness of ZnO thin films by electroless deposition versus deposition time. The rate of deposition is 3−4 nm/min.

Figure 10 shows SEM images of vertically aligned ZnO nanowires deposited on plasma-etched Au patches. The ZnO nanowires were deposited following the recipe of Greene et al.[26] First, a ZnO seed growth step was performed to generate hexagonal wurtzite seeds of ZnO. This step was essential, because ZnO nanowires did not nucleate heterogeneously on the plasma-etched areas of the Au substrate in the nutrient solution, and only homogeneous nucleation in the solution occurred. The substrates were kept floating on the surface of the nutrient solution, with the ZnO seeded side facing downward into the solution. This was essential to avoid any homogeneously grown ZnO nanowires from depositing on the substrate. The ZnO nanowires were grown vertically downward, following the crystal orientation of the ZnO seeds. The XRD data confirmed the preferential [0001] growth direction of wurtzite ZnO. The growth rate of the nanowires was ∼100 nm/h. We grew nanowires for periods of 1 to 24 h. It was necessary to replace the nutrient solution after 10 h to maintain a constant growth rate, in view of the considerable reduction of Zn^{2+} ion concentration in the solution due to consumption by growth.

3.2.3. Electroless Deposition of Ag. Figure 11a,b shows Ag micropatterns formed over ODT patterned thin Au catalyst film. The deposition time was ∼10 min for a thickness of 100 nm. The growth rate can be controlled by the dilution of the Ag enhancer solution. Film thickness can be controlled by the deposition time.

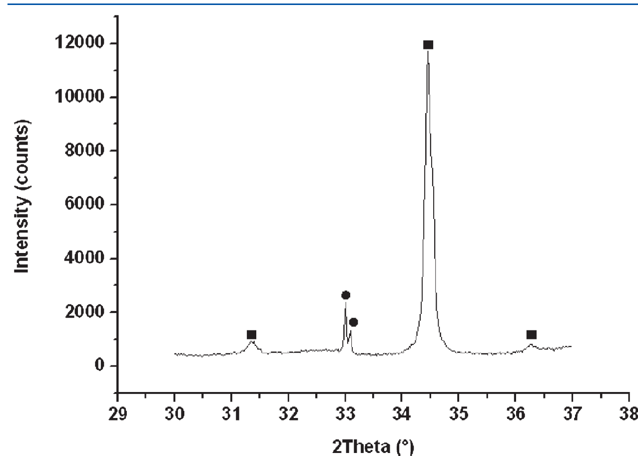

Figure 8. XRD pattern of ZnO thin films grown at 65 °C. The peak at $2\theta = 34.4°$ corresponds to the (0002) reflection of the ZnO wurtzite structure. The squares represent ZnO pattern peaks and the circles represent substrate peaks. The double peak at $2\theta = 33°$ is from the silicon substrate. The splitting of the silicon peak is due to the presence of K_α and K_β radiation.

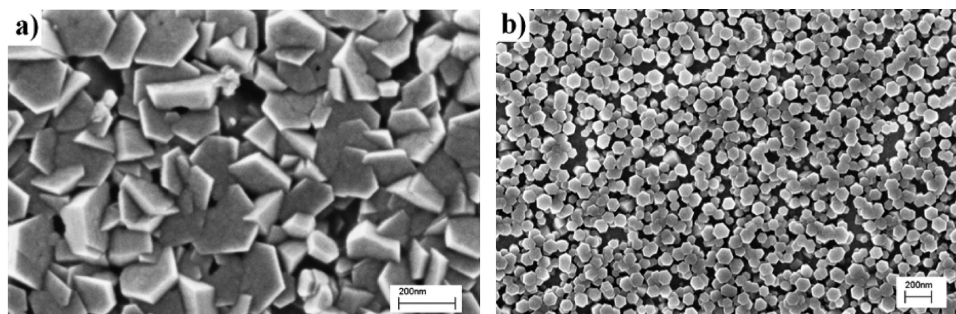

Figure 7. Morphology of ZnO thin films grown by electroless deposition: (a) 55 °C; (b) 65 °C.

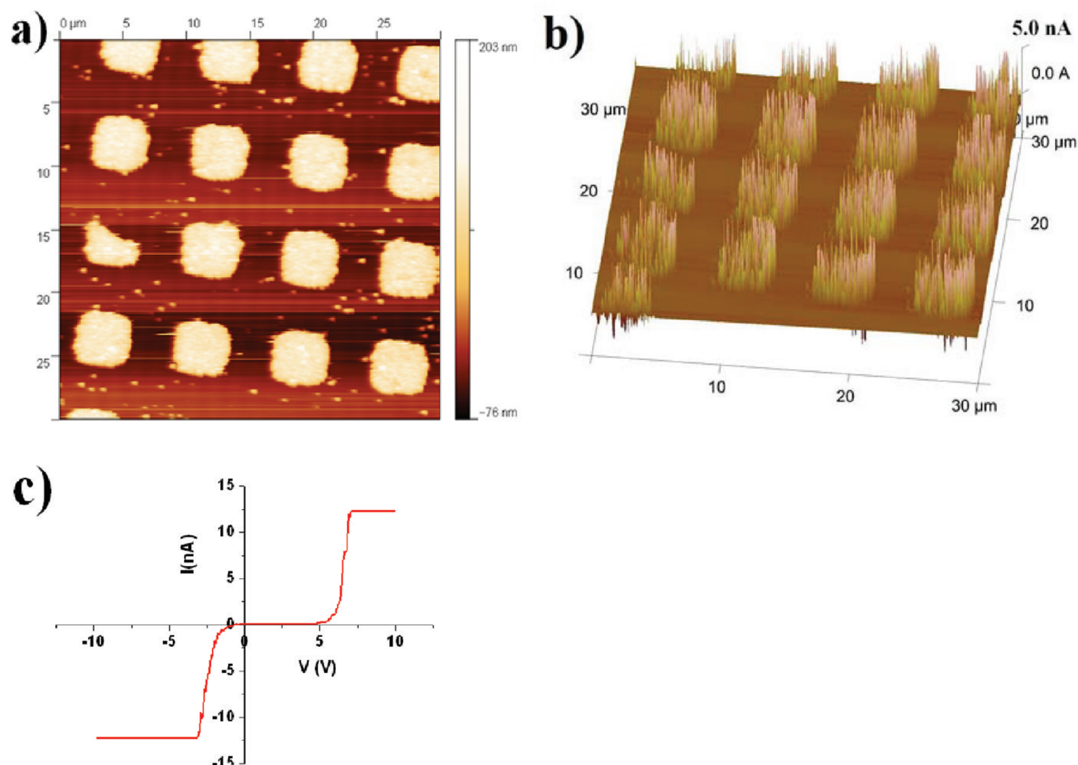

Figure 9. AFM contact-mode image, contact-mode height profile, TUNA AFM conductivity map, and TUNA $I-V$ characteristics of isolated electroless ZnO pattern.

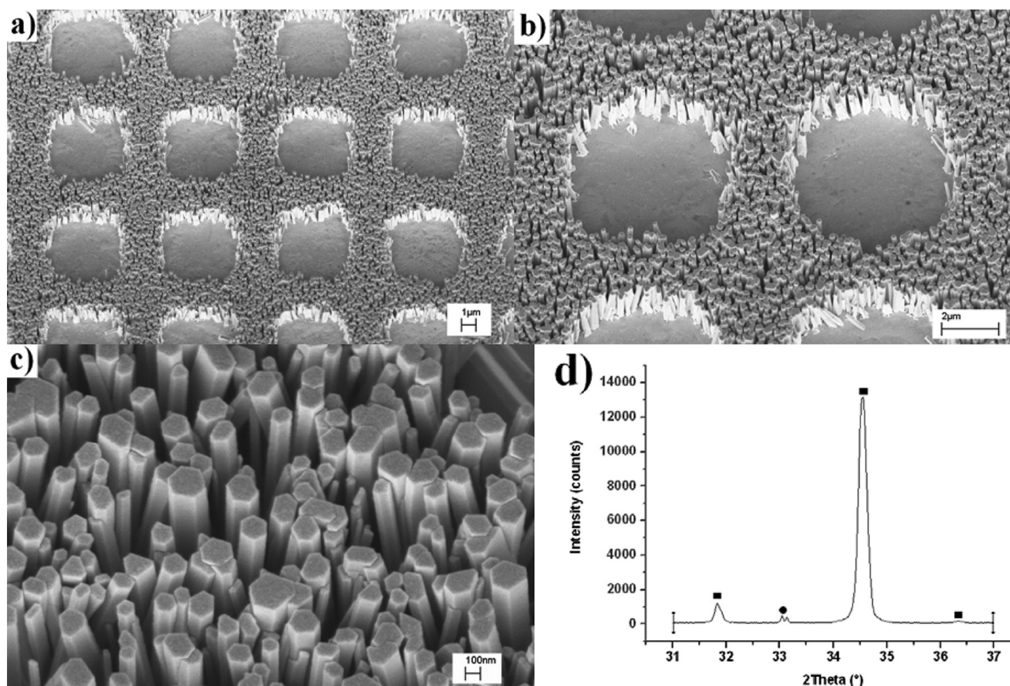

Figure 10. (a−c) SEM images of ZnO nanowires grown on plasma-etched regions of the Au film at different magnifications. Growth time was 15 h. The nanowires were approximately 1.5 μm long. (d) XRD pattern of ZnO nanowire patterns grown at 75 °C. The peak at 2θ = 34.4° corresponds to the (0002) reflection of the ZnO wurtzite structure. The black squares designate ZnO pattern peaks and the black circles indicate substrate peaks. The double peak at 2θ = 33° is from the silicon substrate. The splitting of the silicon peak is due to the presence of K_α and K_β radiation.

3.2.4. Electrodeposition of ZnO and Ni. Figure 11c,d shows SEM images of electrodeposited Ni patterns on etch-patterned Au films. Figure 11e,f shows AFM and SEM images of ZnO patterns deposited on etch-patterned Au thin films. The electrodeposition

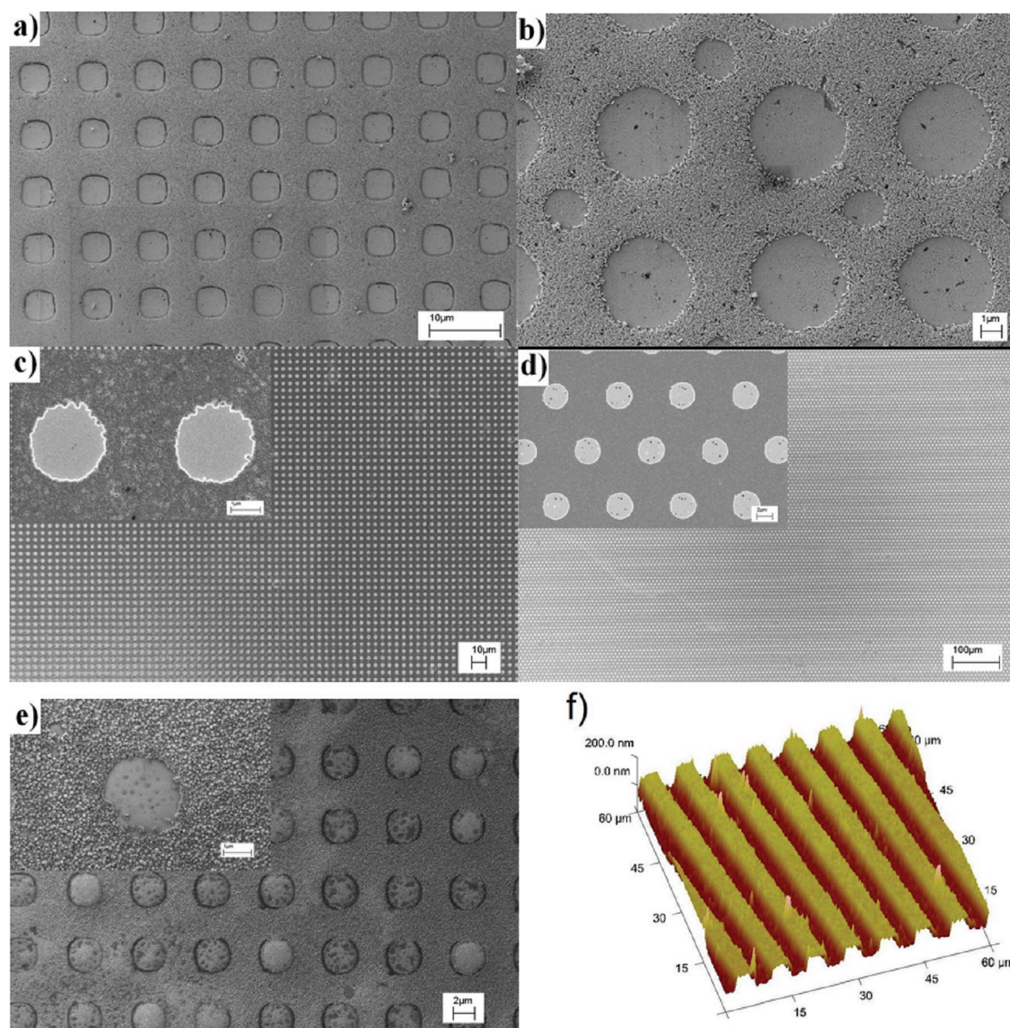

Figure 11. SEM images of patterned materials. (a) Electroless Ag micropatterns formed on plasma-etched Au film with square array of square holes (width 5.3 μm; spacing 2.8 μm); (b) electroless Ag film with a square array of circular pits (diameter large circles 4.5 μm; diameter small circles 2.5 μm; minimum spacing between circles ~2 μm); (c) electrodeposited Ni square array of circular pits (diameter 2.5 μm, spacing 2.5 μm); (d) electrodeposited Ni hexagonal array of circular pits (diameter 3.3 μm, spacing 4.8 μm); (e) electrodeposited ZnO circular pit pattern (diameter and spacing 3 μm); (f) 3D tapping-mode AFM image of electrodeposited ZnO line patterns with line width and spacing ~4 μm.

process was in both cases carried out at constant voltage for short intervals of time, i.e., 10−60 s. The deposition rate of ZnO was ~4 nm/min. The ZnO patterns shown were grown for 30 s, and the thickness of the deposited film was ~120 nm.

4. CONCLUSIONS

Channel-diffused plasma etching is a simple, cost-effective, and efficient technique to prepattern substrates for subsequent site-controlled deposition of functional metal and oxide materials such as ZnO films and nanowires, and Ag or Ni films by electrodeposition, electroless deposition, or solution-phase deposition. Both interconnected patterns and isolated features were deposited. PDMS stamps with a connected channel structure provided the best results due to the fast diffusion of oxygen plasma that is possible in such structures. Channel-diffused plasma etching is a time-dependent process. During the etching process, we observed a roughened Au film after plasma exposure, which stimulated the nucleation of ZnO during the subsequent electroless deposition process. The deposited ZnO thin films and nanowire micropatterns have semiconducting properties. The process could be more efficient and faster by engineering more plasma inlets from the sides and at the top of the PDMS channel mask.

■ AUTHOR INFORMATION

Corresponding Author

*E-mail: J.E.tenElshof@utwente.nl.

■ ACKNOWLEDGMENT

Financial support of NWO-STW in the framework of the Vernieuwingsimpuls programme (VIDI) is acknowledged.

■ REFERENCES

(1) Carr, D. W.; Lercel, M. J.; Whelan, C. S.; Craighead, H. G.; Seshadri, K.; Allara, D. L. *J. Vac. Sci. Technol., A* **1997**, *15*, 1446–1450.

(2) Pesika, N. S.; Radisic, A.; Stebe, K. J.; Searson, P. C. *Nano Lett.* **2006**, *6*, 1023–1026.

(3) Hsu, C.-H.; Yeh, M.-C.; Lo, K.-L.; Chen, L.-J. *Langmuir* **2007**, *23*, 12111–12118.

(4) Maury, P.; Peter, M.; Mahalingam, V.; Reinhoudt, D. N.; Huskens, J. *Adv. Funct. Mater.* **2005**, *15*, 451–457.
(5) Hoff, J. D.; Cheng, L.-J.; Meyhofer, E.; Guo, L. J.; Hunt, A. J. *Nano Lett.* **2004**, *4*, 853–857.
(6) Dulcey, C. S.; Georger, J. H.; Krauthamer, V.; Stenger, D. A.; Fare, T. L.; Calvert, J. M. *Science* **1991**, *252*, 551–554.
(7) Greg, G.; Scott, W.; Joe, B.; Michael, J. T. *Appl. Phys. Lett.* **1994**, *65*, 534–536.
(8) Lercel, M. J.; Tiberio, R. C.; Chapman, P. F.; Craighead, H. G.; Sheen, C. W.; Parikh, A. N.; Allara, D. L. *J. Vac. Sci. Technol., B* **1993**, *11*, 2823–2828.
(9) Jeon, N. L.; Finnie, K.; Branshaw, K.; Nuzzo, R. G. *Langmuir* **1997**, *13*, 3382–3391.
(10) Ginger, D. S.; Zhang, H.; Mirkin, C. A. *Angew. Chem., Int. Ed.* **2004**, *43*, 30–45.
(11) Maoz, R.; Frydman, E.; Cohen, S. R.; Sagiv, J. *Adv. Mater.* **2000**, *12*, 424–429.
(12) de la Rica, R.; Baldi, A.; Mendoza, E.; Paulo, Á. S.; Llobera, A.; Fernández-Sánchez, C. *Small* **2008**, *4*, 1076–1079.
(13) George, A.; Blank, D. H. A.; ten Elshof, J. E. *Langmuir* **2009**, *25*, 13298–13301.
(14) Xu, S.; Liu, G.-y. *Langmuir* **1997**, *13*, 127–129.
(15) Biebuyck, H. A.; Larsen, N. B.; Delamarche, E.; Michel, B. *IBM J. Res. Dev.* **1997**, *41*, 159–170.
(16) Delamarche, E.; Schmid, H.; Bietsch, A.; Larsen, N. B.; Rothuizen, H.; Michel, B.; Biebuyck, H. *J. Phys. Chem. B* **1998**, *102*, 3324–3334.
(17) Dameron, A. A.; Hampton, J. R.; Smith, R. K.; Mullen, T. J.; Gillmor, S. D.; Weiss, P. S. *Nano Lett.* **2005**, *5*, 1834–1837.
(18) Masuda, Y.; Kinoshita, N.; Sato, F.; Koumoto, K. *Cryst. Growth Des.* **2006**, *6*, 75–78.
(19) Masuda, Y.; Seo, W. S.; Koumoto, K. *Langmuir* **2001**, *17*, 4876–4880.
(20) Masuda, Y.; Ieda, S.; Koumoto, K. *Langmuir* **2003**, *19*, 4415–4419.
(21) Shirahata, N.; Masuda, Y.; Yonezawa, T.; Koumoto, K. *Langmuir* **2002**, *18*, 10379–10385.
(22) Saito, N.; Haneda, H.; Komatsu, M.; Koumoto, K. *J. Electrochem. Soc.* **2006**, *153*, C170–C175.
(23) Saito, N.; Haneda, H.; Sekiguchi, T.; Ohashi, N.; Sakaguchi, I.; Koumoto, K. *Adv. Mater.* **2002**, *14*, 418–421.
(24) Lin, M.-H.; Chen, C.-F.; Shiu, H.-W.; Chen, C.-H.; Gwo, S. *J. Am. Chem. Soc.* **2009**, *131*, 10984–10991.
(25) Izaki, M.; Omi, T. *J. Electrochem. Soc.* **1997**, *144*, L3–L5.
(26) Greene, L. E.; Law, M.; Goldberger, J.; Kim, F.; Johnson, J. C.; Zhang, Y.; Saykally, R. J.; Yang, P. *Angew. Chem., Int. Ed.* **2003**, *42*, 3031–3034.
(27) Khan, S. U.; Gobel, O. F.; Blank, D. H. A.; ten Elshof, J. E. *ACS Appl. Mater. Interfaces* **2009**, *1*, 2250–2255.
(28) Gobel, O. F.; Blank, D. H. A.; ten Elshof, J. E. *ACS Appl. Mater. Interfaces* **2010**, *2*, 536–543.
(29) ten Elshof, J. E.; Khan, S. U.; Göbel, O. F. *J. Eur. Ceram. Soc.* **2010**, *30*, 1555–1577.
(30) Wang, Z. L.; Song, J. *Science* **2006**, *312*, 242246.
(31) Huang, M. H.; Mao, S.; Feick, H.; Yan, H.; Wu, Y.; Kind, H.; Weber, E.; Russo, R.; Yang, P. *Science* **2001**, *292*, 1897–1899.
(32) Liao, L.; Lu, H. B.; Li, J. C.; Liu, C.; Fu, D. J.; Liu, Y. L. *Appl. Phys. Lett.* **2007**, *91*, 173110–173110−3.
(33) Law, M.; Greene, L. E.; Johnson, J. C.; Saykally, R.; Yang, P. *Nat. Mater.* **2005**, *4*, 455–459.
(34) Huang, Y.; Zhang, Y.; Gu, Y.; Bai, X.; Qi, J.; Liao, Q.; Liu, J. *J. Phys. Chem. C* **2007**, *111*, 9039–9043.
(35) Yeh, P. H.; Li, Z.; Wang, Z. L. *Adv. Mater.* **2009**, *21*, 4975–4978.
(36) Maas, M. G.; Rodijk, E. J. B.; Maijenburg, A. W.; Blank, D. H. A.; Ten Elshof, J. E. *J. Mater. Res.* **2011**, DOI: 10.1557/jmr.2011.93
(37) Veeco AFM manual, Application Modules, Nanoscope V7-B (004−1020−000).